iScience

CellPress
OPEN ACCESS

Article

Gate-controlled gas sensor utilizing 1D–2D hybrid nanowires network

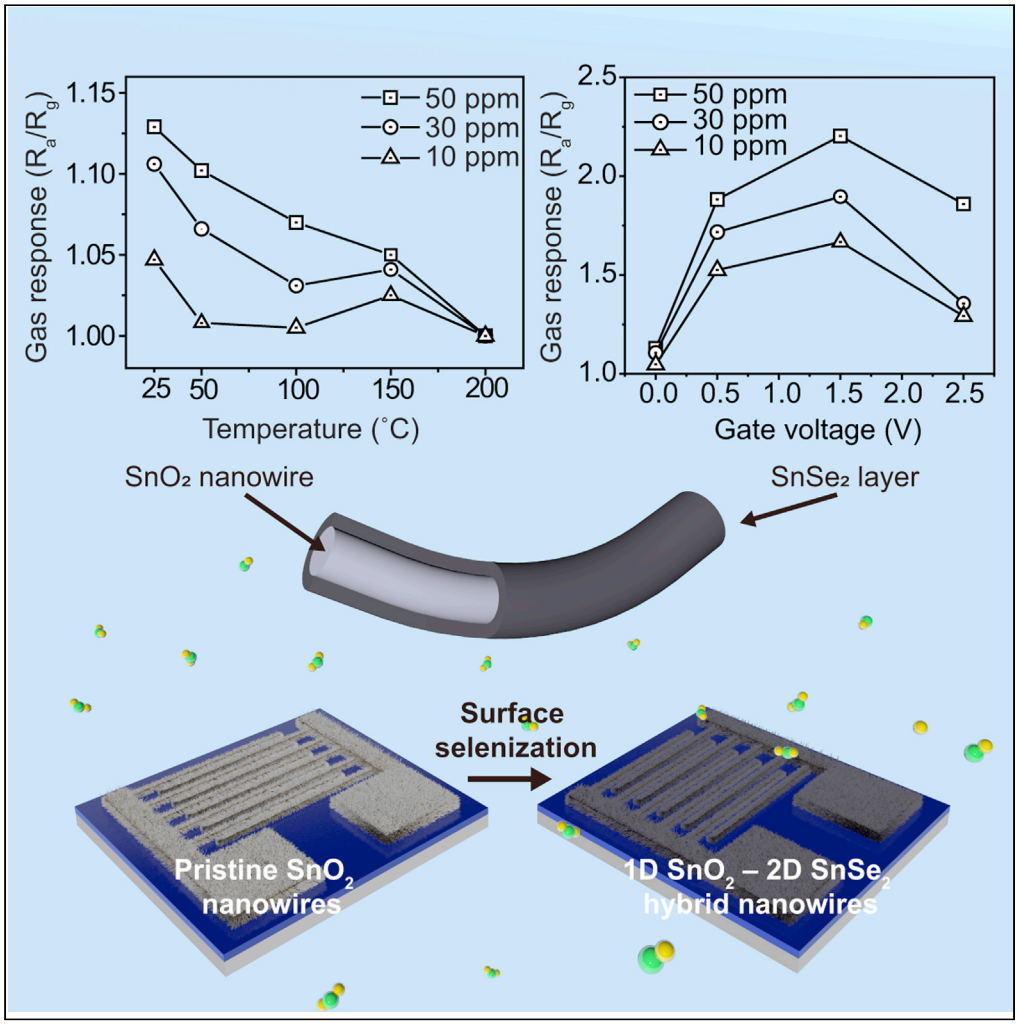

Juyeon Seo, Seung Hyun Nam, Moonsang Lee, ..., Sang Sub Kim, Un Jeong Kim, Myung Gwan Hahm

sangsub@inha.ac.kr (S.S.K.)
ujjane.kim@samsung.com (U.J.K.)
mghahm@inha.ac.kr (M.G.H.)

Highlights

1D SnO_2 Nanowire–2D $SnSe_2$ Heterostructure-based Gas Sensor

Selectivity for NO_2 gas at room temperature

Improve the sensing characteristics through a large effective reaction area

Controlling the gate bias enhances carrier movement and improves sensing performance

Seo et al., iScience 25, 103660
January 21, 2022
https://doi.org/10.1016/j.isci.2021.103660

iScience

CellPress
OPEN ACCESS

Article

Gate-controlled gas sensor utilizing 1D–2D hybrid nanowires network

Juyeon Seo,[1,6] Seung Hyun Nam,[1,6] Moonsang Lee,[1,6] Jin-Young Kim,[1] Seung Gyu Kim,[1] Changkyoo Park,[2] Dong-Woo Seo,[3] Young Lae Kim,[4] Sang Sub Kim,[1,*] Un Jeong Kim,[5,*] and Myung Gwan Hahm[1,7,*]

SUMMARY

Novel gas sensors that work at room temperature are attracting attention due to their low energy consumption and stability in the presence of toxic gases. However, the development of sensing characteristics at room temperature is still a primary challenge. Diverse reaction pathways and low adsorption energy for gas molecules are required to fabricate a gas sensor that works at room temperature with high sensitivity, selectivity, and efficiency. Therefore, we enhanced the gas sensing performance at room temperature by constructing hybridized nanostructure of 1D–2D hybrid of $SnSe_2$ layers and SnO_2 nanowire networks and by controlling the back-gate bias (V_g = 1.5 V). The response time was dramatically reduced by lowering the energy barrier for the adsorption on the reactive sites, which are controlled by the back gate. Consequently, we believe that this research could contribute to improving the performance of gas sensors that work at room temperature.

INTRODUCTION

The control of the reaction sites and charge concentration of a sensing material is a critical factor that determines gas sensing performance at room temperature. Metal oxide semiconductors have been used as a representative sensing material for chemiresistive gas sensors due to their good chemical stability and sensitivity. However, their relatively low intrinsic conductivity gives rise to high operating temperature (above 100°C–200°C), which hinders the use of these materials in an energy-efficient gas sensor (Ahn et al., 2009; Cao et al., 2014; Choi et al., 2008). Thus, optimization of the reaction sites for the carrier transfer and its concentration is crucial to achieve low-temperature operation.

Two-dimensional (2D) semiconductors have attracted significant interest for active sensing materials. Their ultrathin thickness contributes a high specific surface area and a large number of reactive sites for charge transfer between gas molecules and the sensing material (Dey, 2018; Donarelli and Ottaviano, 2018; McAlpine et al., 2007; Shalev, 2017; Yan et al., 2020). Based on these structural features, low operating temperature (near room temperature) has been reported for sensors based on 2D materials, especially transition metal dichalcogenides (TMDs), such as MoS_2, WSe_2, and $SnSe_2$ (Cho et al., 2015, 2016; Choi et al., 2017; Cui et al., 2020; Dey, 2018; Kang et al., 2019; Moumen et al., 2021; Ricciardella et al., 2017; Liu et al., 2021). However, there are several challenges that should be addressed, such as irreversible sensing behavior, slow response and recovery time, and high oxidation rate at high operating temperature (Camargo Moreira et al., 2019; Li et al., 2012; Yan et al., 2018). Therefore, constructing a nanostructure with a large effective reaction area (i.e., specific surface, crystal defects, etc.) and well-optimized carrier concentration is highly desirable to improve the sensing characteristics at low temperature (Shalev, 2017).

Recently, heterostructures consisting of two different semiconducting nanomaterials, such as 2D semiconducting TMDs and metal oxide semiconductors, have been investigated as promising active sensing materials for chemiresistive gas sensors (Kumar et al., 2020; Paolucci et al., 2020; Zhao et al., 2018). Owing to their different electronic band structures, the effective charge concentration can be modulated by the charge transfer between the two atomic layers (Gu et al., 2017; Hao et al., 2018). This contributes to the enhancement of the chemisorption of oxygen, which is one of the major factors that determine the sensing response at low operating temperatures. In addition, reactive sites are increased *via* the large specific surface area obtained by the formation of the heterostructure, which facilitates the chemical interaction between the gas molecules and the sensing materials. This leads to improved response time and reversible

[1]Department of Materials Science and Engineering, Inha University, 100 Inha-ro, Michuhol-gu, Incheon 22212, Republic of Korea

[2]Department of Laser and Electron Beam Technologies, Korea Institute of Machinery and Materials, Daejeon 34103, Republic of Korea

[3]Korea Institute of Civil Engineering and Building Technology, 283 Goyangdae-ro, Goyang-Si, Gyeonggi-Do 10223, Republic of Korea

[4]Department of Electronic Engineering, Gangneung-Wonju National University, Gangneung 25457, Republic of Korea

[5]Advanced Sensor Laboratory, Samsung Advanced Institute of Technology, Suwon 443-803, Republic of Korea

[6]These authors are contributed equally

[7]Lead contact

*Correspondence: sangsub@inha.ac.kr (S.S.K.), ujjane.kim@samsung.com (U.J.K.), mghahm@inha.ac.kr (M.G.H.)

https://doi.org/10.1016/j.isci.2021.103660

behavior of the sensor at room temperature (Han et al., 2018; Lee et al., 2018; Li et al., 2017; Wang et al., 2021).

In this work, we investigated the gas sensing characteristics of a 1D–2D hybrid network structure with SnO_2 nanowires and $SnSe_2$ layers. The surface of the pristine SnO_2 nanowires was shallowly converted into ultrathin $SnSe_2$ by chemical vapor deposition (CVD). The hybridized nanowire networks showed increased chemisorption of oxygen ions after selenization, which led to electron transfer from SnO_2 to the $SnSe_2$ layer. The formation of the ultrathin $SnSe_2$ also provided carrier accumulation on the surface of the nanowires network, which resulted in stable NO_2 sensing performance at room temperature. As a result, oxygen molecules adsorption is facilitated by large electron density of $SnSe_2$ surface which is accumulated from SnO_2 to $SnSe_2$.

The influence of the gate voltage on the detection of NO_2 gas is demonstrated using a highly doped Si as a back gate. The adsorption energy was reduced by applied gate bias, which facilitated the chemical reaction between the surface of the sensing material and gas molecules. As a result, enhanced response performance with 50 ppm of NO_2 could be achieved at room temperature.

RESULTS AND DISCUSSION

Creation of 1D–2D hybrid nanowires network *via* chemical vapor deposition

Pristine SnO_2 nanowires were prepared by a vapor-liquid-solid (VLS) method and selenized using a direct selenization process based on CVD (Figure 1A). First, Au (3 nm)/Pt (300 nm)/Ti (50 nm) interdigitated electrodes with 20-μm width and spacing were prepared, and then, SnO_2 nanowires were selectively grown *via* the VLS growth method at 900°C for 30 min. The resulting ultrathin $SnSe_2$ was synthesized on the surface of the SnO_2 nanowires network at 550°C for 30 min using Se powder as the Se precursor (see STAR Methods for details).

Field emission scanning electron microscopy (FESEM) and field emission transmission electron microscopy (FETEM) were conducted to confirm the morphology and microstructure of SnO_2 nanowires after the surface selenization process. The Au layer was used for the selective growth of SnO_2 nanowires, so the SnO_2 nanowires were grown on only the interdigitated electrodes and formed a network structure. As shown in Figure 1B, this networked structure of SnO_2 nanowires is maintained after the CVD-based selenization process.

Figures 1C and 1D present low- and high-magnification FESEM images of the 1D SnO_2–2D $SnSe_2$ hybrid nanowire network. It is clear that highly dense nanowires are randomly oriented with 40- to 50-nm diameter. Figure 1E shows an FETEM image of the 1D SnO_2–2D $SnSe_2$ hybrid nanowire network. An ultrathin $SnSe_2$ layer with thickness of a few nanometers was formed uniformly on the surface of as-grown SnO_2 nanowires (Figure S1). The scanning TEM (STEM) image and corresponding energy-dispersive X-ray spectroscopy (EDS) mapping images of the SnO_2 nanowires network with the $SnSe_2$ layer show the coexistence of Sn, O, and Se over the whole nanowires network, as well as the distribution of Se throughout the surface of the SnO_2 nanowires (Figure 1F) (Zhou et al., 2015).

Structural and chemical characterizations of the 1D SnO_2–2D $SnSe_2$ hybrid nanowires network

X-ray diffraction (XRD) was conducted to investigate the crystal structure of the 1D–2D hybrid nanowires. Figure 2A shows the XRD spectra of as-grown SnO_2 nanowires before and after the CVD-based surface selenization. The XRD pattern of the pristine SnO_2 nanowires shows multiple peaks located at 26.4°, 33.7°, 51.8°, and 54.8°, which correspond to the (110), (101), (211), and (200) planes of SnO_2, respectively (JCPDS 41-1445). After the surface selenization, diffraction peaks of $SnSe_2$ start to appear with the peaks observed in the pristine SnO_2 nanowires. The peaks at around 29.6°, 30.6°, 43.5°, and 47.5° are assigned to the (002), (011), (003), and (110) planes of $SnSe_2$, respectively. This indicates that the ultrathin $SnSe_2$ was successfully synthesized on the surface of SnO_2 nanowire networks.

As shown in Figure 2B, Raman spectroscopy was conducted to confirm the atomic bonding structure of the 1D SnO_2–2D $SnSe_2$ hybrid nanowires. The Raman spectrum of the pristine SnO_2 nanowires shows three characteristic peaks at around 474, 633, and 776 cm^{-1}. These are respectively related to the E_g, A_{1g}, and B_{2g} modes of the SnO_2 nanowires, which have rutile tetragonal structure (Chen et al., 2017; Costa et al.,

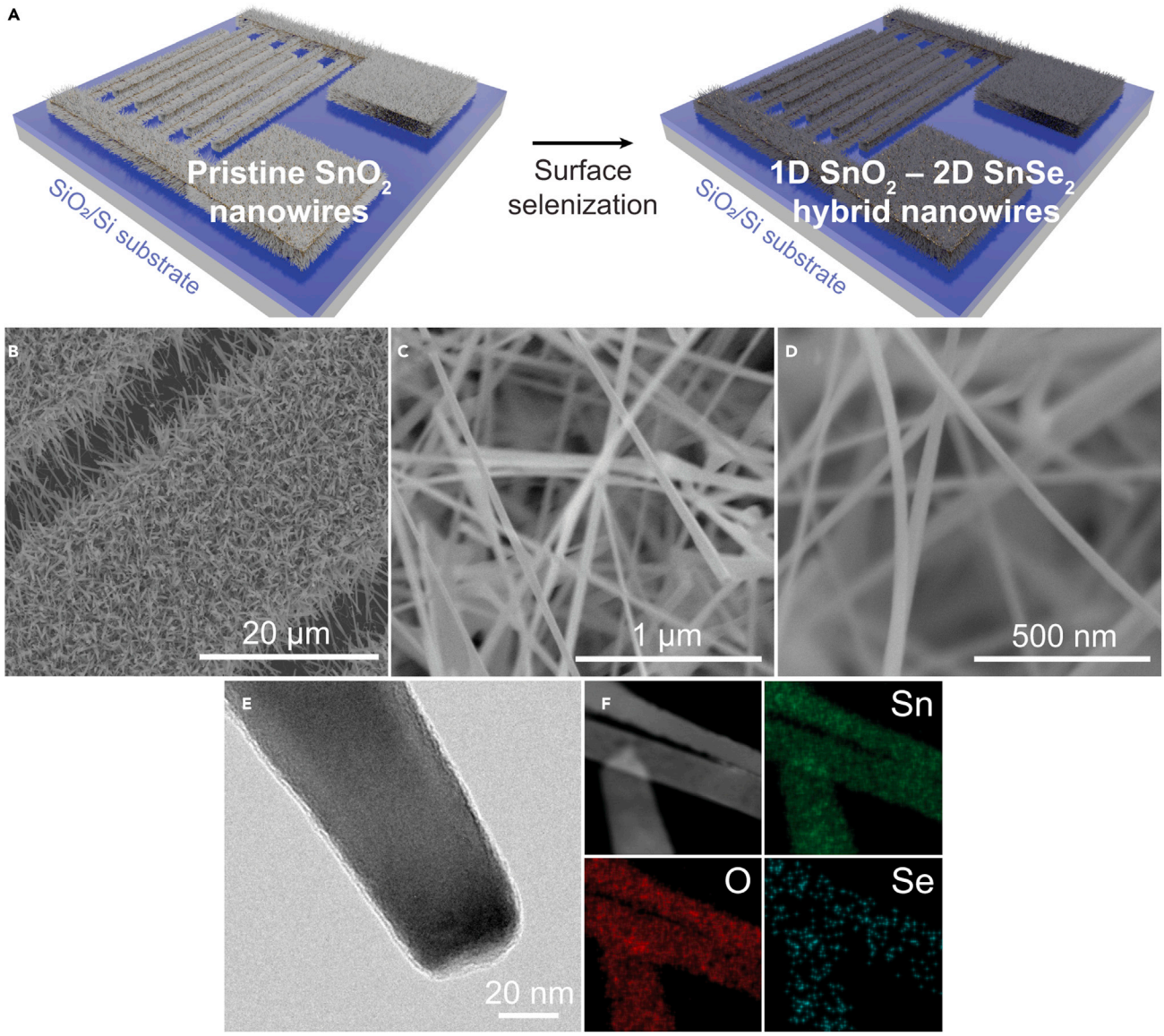

Figure 1. Preparation and structural characterization of 1D SnO_2–2D $SnSe_2$hybrid nanowire network

(A) Illustration showing the CVD-based selenization process of pristine SnO_2 nanowires.

(B) FESEM image of 1D SnO_2–2D $SnSe_2$ nanowire network selectively grown on Au/Pt/Ti interdigitated electrodes.

(C and D) FESEM images of SnO_2 nanowires with ultrathin $SnSe_2$ under (C) low and (D) high magnification.

(E) FETEM image of SnO_2 nanowire after the selenization process showing ultrathin shell of $SnSe_2$ formed on SnO_2 nanowire.

(F) STEM-HAADF image with corresponding EDS mapping images of Sn (green), O (red), and Se (blue).

2018). Compared to the pristine SnO_2 nanowires, two prominent Raman vibrational modes of $SnSe_2$ are exhibited at 116.6 and 184.7 cm^{-1} after the selenization. The Raman peaks are ascribed to the in-plane A_{1g} mode and the out-of-plane E_g mode, respectively (see inset of Figure 2B) (Shao et al., 2018). The weak intensity of the E_g mode is attributed to the few scattering centers in the few-layered $SnSe_2$ (An et al., 2020). The frequencies of these two characteristic Raman peaks depend on the number of layers of $SnSe_2$ (Gonzalez and Oleynik, 2016; Zhang et al., 2018). Thus, the crystalline $SnSe_2$ is well formed on the surface of SnO_2 nanowires with fewer than 5 layers, which agrees with the FETEM (Figure 1E) and XRD results (Figure 2A).

The in-plane A_{1g} vibrational mode of SnO_2 also shows relatively weak peak intensity, suggesting the presence of SnO_2 nanowires below the selenized surface. However, there is a red shift of the A_{1g} mode from 633 to 631 cm^{-1}, implying that there is incorporation of oxygen into the crystal lattice (Li et al., 2020). This can

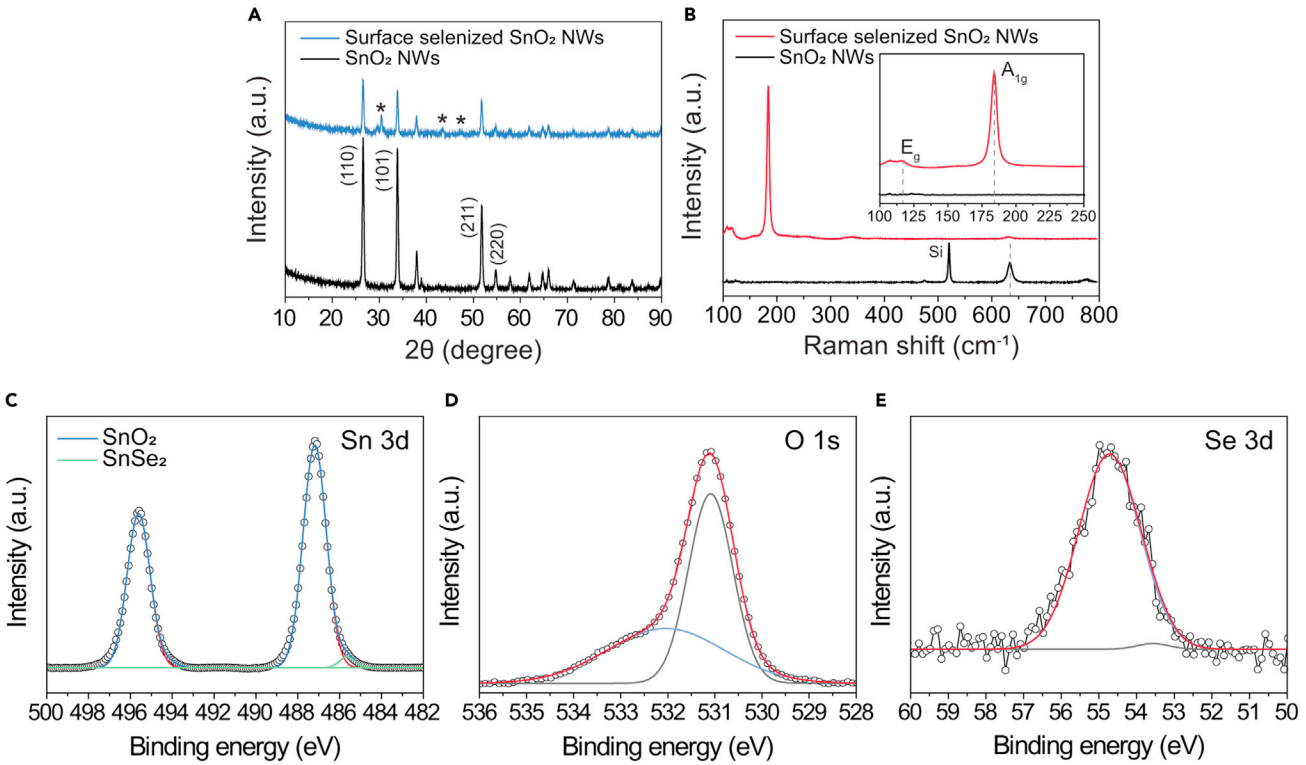

Figure 2. Structural and chemical characterizations of 1D SnO_2–2D $SnSe_2$hybrid nanowire network

(A) XRD spectra of pristine SnO_2 nanowire (top) and SnO_2 nanowires with ultrathin $SnSe_2$ (bottom).

(B) Raman spectra of SnO_2 nanowires before (top) and after (bottom) selenization process. The inset shows the magnified Raman spectra in the range of 100–250 cm^{-1}, in which two characteristic Raman peaks of 2D $SnSe_2$ indicate the successful formation of ultrathin $SnSe_2$ layer on the surface of the SnO_2 nanowires.

(C–E) XPS spectra of (C) Sn 3d, (D) O 1s, and (E) Se 3d for the1D SnO_2–2D $SnSe_2$ heterostructure.

change the interaction of the planar lattice, thus affecting the in-plane vibrational mode. Moreover, a weak Raman peak is observed around 107 cm^{-1}, which corresponds to the B_{3g} mode of SnSe (Jiang et al., 2017). This indicates the presence of a partially selenized region in the as-prepared nanowires.

As shown in Figures 2C–2E, the valence state of each element on the surface of the selenized SnO_2 nanowires was also investigated by X-ray photoelectron spectroscopy (XPS). The high-resolution Sn 3d spectrum in Figure 2C exhibits two sets of core levels of Sn, which correspond to Sn-O bonding in SnO_2 (Sn $3d_{5/2}$: 487.19 eV, Sn $3d_{3/2}$: 495.6 eV) and Sn-Se bonding in $SnSe_2$ (Sn $3d_{5/2}$: 485.63 eV, Sn $3d_{3/2}$: 494.16 eV) (Rai et al., 2019; Wang et al., 2021). The weak intensity of the peaks of Sn-Se bonding indicates the presence of the ultrathin $SnSe_2$ layer on the surface of SnO_2 nanowires.

In the XPS spectrum of O 1s (Figure 2D), two peaks at 531.10 and 532.04 eV are associated with O-Sn bonding in SnO_2 and chemisorbed oxygen ions, respectively. As shown in Figure S2, the concentration of chemisorbed oxygen ions is increased after the selenization process. This clearly indicates that the CVD-based surface selenization method can result in the increase of the oxygen chemisorbed on the surface of the nanowires.

The XPS spectrum of Se 3d in Figure 2E can be deconvoluted into two peaks, which are assigned to Se $3d_{5/2}$ (53.57 eV) and Se $3d_{3/2}$ (54.72 eV) (Lu et al., 2021). These XPS results are consistent with the EDS data in Figure 1F, implying the coexistence of Sn, O, and Se in as-grown samples. Based on these results, it can be concluded that the CVD process successfully selenized the surface of the rutile SnO_2 nanowires with ultrathin $SnSe_2$, which had good crystallinity. The formation of a 2D $SnSe_2$ layer on the surface of 1D SnO_2 nanowires increases the interaction with the atmosphere, which can be expected to enhance the gas sensing performance.

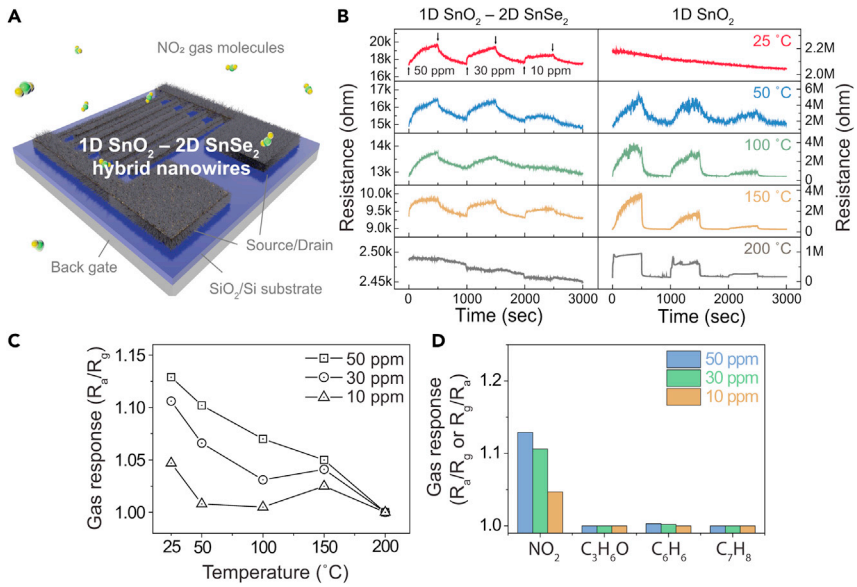

Figure 3. Gas sensing characteristics of 1D SnO_2–2D $SnSe_2$hybrid nanowire network-based gas sensor for NO_2gas

(A) Illustration of NO_2 gas sensor based on SnO_2 nanowires with ultrathin $SnSe_2$.

(B) Dynamic resistance curves of pristine SnO_2 nanowires (right) and 1D SnO_2–2D $SnSe_2$ heterostructure (left)-based gas sensor to different NO_2 gas concentrations of 10–50 ppm at different temperatures (room temperature – 200°C).

(C) Comparative analysis of NO_2 gas sensitivity at different operating temperatures and gas concentrations of 10–50 ppm.

(D) Comparison of gas sensing response of the 1D SnO_2 nanowire–2D $SnSe_2$ heterostructure-based gas sensor against various gases (NO_2, C_3H_6O, C_6H_6, and C_7H_8) at different gas concentration from 10 to 50 ppm.

Gas sensing characteristics of the 1D SnO_2nanowire–2D $SnSe_2$ heterostructure-based gas sensor for NO_2 gas

A schematic drawing of the 1D SnO_2nanowire–2D $SnSe_2$-based gas sensor is shown in Figure 3A. To investigate the capabilities of the ultrathin 2D $SnSe_2$ layers on 1D SnO_2 nanowires, the dynamic resistance responses of the SnO_2 nanowires were measured before and after the surface selenization at different NO_2 concentrations with different temperatures. The gas responses were calculated by $S = R_g/R_a$ in oxidizing gas and R_a/R_g in reducing gas, where R_a and R_g are the resistances of the sensor in air and in the presence of the target gas, respectively.

The transient resistance curves of the 1D–2D heterostructure (left) and pristine SnO_2 nanowires network (right) in Figure 3B show the resistance in response to the analyte gas (NO_2). NO_2 gas molecules act as electron acceptors that pick the electrons out of the surface of sensing materials (Cheng et al., 2016; Lee et al., 2018). When the gas molecules are adsorbed onto the surface of the 1D–2D heterostructure and the pristine SnO_2 nanowires network, the electrons in the conduction band are extracted, decreasing the concentration of carriers, and broadening the depletion layer (Feng et al., 2014). This contributes to the formation of a depletion layer through the surface of the nanowires, which increases the resistance of the sensor. The bare SnO_2 and 1D SnO_2–2D $SnSe_2$ nanowire networks have n-type semiconducting behavior (Sun et al., 2012).

The 1D SnO_2–2D $SnSe_2$ nanowire heterostructures clearly exhibited a very good response at room temperature, while there was no response to NO_2 gas in the gas sensor based on a pristine SnO_2 nanowires network (Figures 3B and S3). The formation of the hybrid of 1D SnO_2 and 2D $SnSe_2$ nanowires network improved the sensing characteristics at low temperature compared with the bare SnO_2 nanowires. The resistance variation of the 1D SnO_2 and 2D $SnSe_2$ nanowires network gas sensor reaches its maximum at room temperature. As the temperature increases with increments of 50°C from room temperature to 150°C, the resistance variation of the sensor with the 1D–2D hybrid structure decreases by 2, 1.5, 1, and 0.5 kΩ, respectively. The recovery of the resistance to its initial value in air was also observed from room temperature to 150°C, implying good reversible behavior of the 1D SnO_2–2D $SnSe_2$ heterostructure-based gas sensor.

Figure 3C shows the dependence of the sensitivity on the operating temperature at three different concentrations (10, 30, and 50 ppm). The sensitivities are proportional to the gas concentration, which is attributed to its dependence on the amount of gas molecules that can react with the sensing material. The maximum value of the gas response was 1.129 at 50 ppm of NO_2 and room temperature. The gas response decreased when the working temperature increased from room temperature to 200°C.

The enhancement of the sensing characteristics at room temperature was ascribed to the accumulation of electrons that are transferred from the as-prepared SnO_2 nanowires on the surface of the $SnSe_2$ layer. When the ultrathin $SnSe_2$ is formed on the surface of SnO_2 nanowire networks, electrons are transferred from SnO_2 to $SnSe_2$ due to the higher bandgap (E_g) and Fermi level (E_f) of the pure SnO_2 than those of $SnSe_2$ (Matysiak et al., 2020; Vemula et al., 2021; Zhou et al., 2015). This creates an interface depletion layer at the SnO_2 and an accumulation layer at the $SnSe_2$, as illustrated in Figure S4.

Oxygen molecules are attracted by the accumulated electrons on the $SnSe_2$ layer, which corresponds to the increase in the chemisorption of oxygen ions, which is consistent with Figure 2D. The increased concentration of the chemisorbed oxygen ions causes the reactions between the NO_2 molecules and adsorbed oxygen ions to multiply, which leads to an improved gas response compared to the gas sensor based on the pristine SnO_2 nanowires. Moreover, the analyte gas can react with defects, resulting in an increase of sensitivity (Thang et al., 2020).

The gas response reaches its maximum at a specific temperature with a mechanism between the available reactive sites at high temperature and slow kinetics at low temperature (Kolmakov et al., 2005; Wang et al., 2010). The speed of chemical reactions is determined by the activation of adsorbed oxygen molecule and lattice ionic oxygen to form active O^{2-}, O^{-}, and mobile O^{2-} species. This phenomenon continues up to a certain operating temperature. And above that, it is difficult to adsorb the exothermic gas molecule by thermal energy, and the gas molecules are easily desorbed, reducing the gas response (Sun et al., 2012; Ping et al., 2017). The number of reactive sites available for the reaction with gas molecules decreases with increasing operating temperature and at higher temperature, the NO_2 gas molecules are easily desorbed and accelerated on surface, which leads to a low response compared with the one at room temperature (Figure 3C) (Ping et al., 2017). Therefore, the ultrathin $SnSe_2$ layers on SnO_2 nanowire networks dramatically enhanced the gas sensing performance at room temperature.

The selectivity of the 1D SnO_2–2D $SnSe_2$ heterostructure-based gas sensor was investigated by measuring the sensing behavior at room temperature in various gases (nitrogen dioxide (NO_2), acetone (C_3H_6O), benzene (C_6H_6), and toluene (C_7H_8)). As shown in Figures 3D and S5, the measure of selective detection to NO_2 gas, S_{NO_2}/S_{gas} (S_{NO2}, response to NO_2 gas, S_{gas}, response to corresponding gas) values can be calculated. The S_{NO2}/S_{gas} values for the 2D $SnSe_2$-based gas sensor to C_3H_6O, C_6H_6, and C_7H_8 gases were 1.129, 1.126, and 1.129 in 50 ppm gas concentration, respectively. These results indicate that S_{NO2}/S_{gas} values are approximately identical to the response to NO_2 gas, indicating that the 2D $SnSe_2$-based gas sensor has selectivity for NO_2 gas (McAlpine et al., 2007; Shehada et al., 2015).

Enhancement of gas sensing performance of the 1D SnO_2nanowire–2D $SnSe_2$ heterostructure-based gas sensor for NO_2 gas by introducing back-gate bias

The typical gas molecule adsorption systems of the surface of the sensing material depend on the energy gap between the Fermi level of metal oxide and the valence band of the gas molecule (Feng et al., 2014; Zhang et al., 2017). When the target gas molecules are attached to the surface of the metal oxide film, carriers on the sensing material surface move into gas molecules by the quantum tunneling. It is because the conduction band of the gas molecule is closer to the Fermi level of the metal oxide than the valence band of the gas molecule. Thus, the energy gap acts as an energy barrier for gas absorption and electron transfer. That means controlling the gate bias causes the Fermi level of the metal oxide to be much closer to the conduction band, lowering the energy barrier and improving gas sensing performance as shown in Figures S4C and S4D (Henning et al., 2015; Khan et al., 2021). Highly doped Si with 300-nm-thick SiO_2 was adopted as a back gate to elucidate the effect of back-gate bias on the sensing characteristics at room temperature, as shown in Figure 3A. The transient resistance to different NO_2 concentrations was measured at room temperature while applying gate bias (i.e., V_g = 0.5, 1.5, and 2.5 V). Compared to the response without gate voltage, the gas sensor shows a very good response (more than 50% higher), even at the lowest NO_2 concentration.

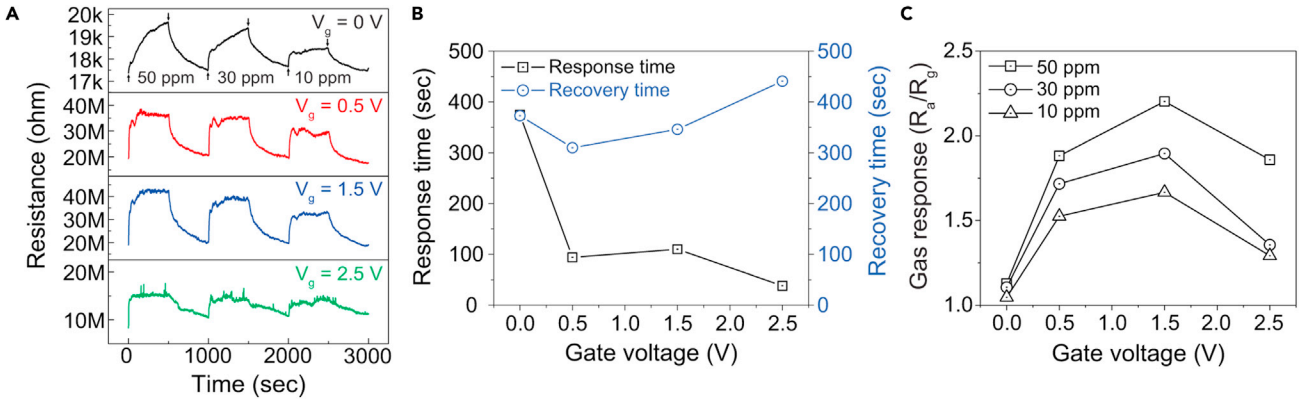

Figure 4. Enhancement in gas sensing performance of 1D SnO_2–2D $SnSe_2$heterostructure-based gas sensor for NO_2 gas by introducing the back-gate bias

(A) Gate-bias dependent dynamic resistance curves of the 1D SnO_2–2D $SnSe_2$ hybrid nanowire networks-based gas sensor to different NO_2 gas concentrations of 10–50 ppm at room temperature. Electrical characteristics measured with V_{DS} = 1 V and V_g = 0, 0.5, 1.0, 1.5, 2.0, 2.5 V.

(B) Response and recovery times as a function of the gate voltage under the exposure to 50 ppm of NO_2 gas at room temperature.

(C) Comparison of NO_2 gas sensing response at different back-gate bias and gas concentrations of 10–50 ppm.

Moreover, as shown in Figure 4B, the response and recovery behavior were also improved with the gate voltage (1.5 V). With a gate voltage of 1.5 V, the recovery time improved from 373 s to 346 s, and the response time was decreased from 375 s to 110 s. This indicates that the energy barrier for the adsorption on the reactive sites would be decreased by the back-gate voltage, which leads to the enhanced reaction between the NO_2 gas molecules and the nanowire surface at room temperature (Hellmich et al., 1997; Vemula et al., 2021). However, the recovery time was still slow, so further research is needed to improve it.

Figure 4C presents the response to different NO_2 gas concentrations as a function of back-gate bias at room temperature. The best gas response achieved at room temperature was 2.2 (R_a/R_g) with exposure to 50 ppm of NO_2 gas at V_g = 1.5 V. This result was almost two times higher than the gas response of 1.13 (R_a/R_g) without applying the gate bias. An increase of the response was also observed with increasing gas concentration, which is attributed to the increased amount of reactive gas molecules. The back-gate voltage contributes to the electron flow by controlling the energy barrier for the adsorption of analyte gas molecules on the surface of 1D–2D hybrid nanowires (Hellmich et al., 1997; Sun et al., 2012; Vemula et al., 2021). As a result, the sensing performance was improved by applying the back-gate voltage.

Conclusions

In summary, a gas sensor was fabricated based on a 1D – 2D hybrid nanowire network that consisted of $SnSe_2$ layers and SnO_2 nanowire, which was obtained using the VLS method and CVD. The sensor had noticeably good gas sensing characteristics at room temperature for NO_2 gas compared to one fabricated with a pristine SnO_2 nanowire network. The sensing characteristics at room temperature were increased by the accumulation of electrons transferred from the SnO_2 nanowires to the surface of the $SnSe_2$ layer.

When back-gate bias (V_g = 1.5 V) was applied to the gas sensor, it showed better sensing performance, including the response time and sensitivity. The enhancement of sensing performance resulted from the energy barrier for the NO_2 gas adsorption on the reactive sites, which was decreased by the back-gate voltage. Considering the sensitivity, response time, and recovery time, the proposed sensor has better performance than a previous NO_2 gas sensor that works at room temperature. Thus, the results could offer insight into the enhancement of sensing performance for gas sensors operating at low temperature, nanostructure design, and diverse applications for future sensing platforms, such as handheld diagnostic tools and smart sensing devices.

Limitations of the study

This study focuses on gas sensing performance of 1D–2D hybrid of $SnSe_2$ layers and SnO_2 nanowire networks at room temperature. Sensing performance is improved compared to previous room temperature work sensors, and the next step is to perform as well as high-temperature operating sensors.

STAR★METHODS

Detailed methods are provided in the online version of this paper and include the following:

- KEY RESOURCES TABLE
- RESOURCE AVAILABILITY
  - Lead contact
  - Materials availability
  - Data and code availability
- EXPERIMENTAL MODEL AND SUBJECT DETAILS
- METHOD DETAILS
  - Synthesis of SnO_2 nanowires
  - Preparation of 1D SnO_2 – 2D $SnSe_2$ hybrid nanowire network
  - Material characterization
  - Gas sensing studies
- QUANTIFICATION AND STATISTICAL ANALYSIS
- ADDITIONAL RESOURCES

SUPPLEMENTAL INFORMATION

Supplemental information can be found online at https://doi.org/10.1016/j.isci.2021.103660.

ACKNOWLEDGMENTS

This work was supported by an INHA University research grant (65355-01).

AUTHOR CONTRIBUTIONS

J. Seo, S. H. Nam, and M. Lee are contributed equally to this work. M. G. Hahm, S. S. Kim, and U. J. Kim conceived and supervised the project. J. Seo, S. H. Nam, M. Lee, and J. Kim prepared and characterized the samples, J. Seo, S. G. Kim, and C. Park performed gas sensor measurements. J. Seo, S. H. Nam, D. Seo, and Y. L. Kim wrote the paper. All authors discussed the results and commented on the manuscript.

DECLARATION OF INTERESTS

The authors declare no competing interests.

Received: August 24, 2021
Revised: November 10, 2021
Accepted: December 16, 2021
Published: January 21, 2022

REFERENCES

Ahn, M.W., Park, K.S., Heo, J.H., Kim, D.W., Choi, K.J., and Park, J.G. (2009). On-chip fabrication of ZnO-nanowire gas sensor with high gas sensitivity. Sensors Actuators B Chem. *138*, 168–173. https://doi.org/10.1016/j.snb.2009.02.008.

An, B., Ma, Y., Zhang, G., You, C., and Zhang, Y. (2020). Controlled synthesis of few-layer $SnSe_2$ by chemical vapor deposition. RSC Adv. *10*, 42157–42163. https://doi.org/10.1039/d0ra08360g.

Camargo Moreira, O.L., Cheng, W.Y., Fuh, H.R., Chien, W.C., Yan, W., Fei, H., Xu, H., Zhang, D., Chen, Y., Zhao, Y., and Lv, Y. (2019). High selectivity gas sensing and charge transfer of $SnSe_2$. ACS Sens *4*, 2546–2552. https://doi.org/10.1021/acssensors.9b01461.

Cao, A., Sudhölter, E.J., and De Smet, L.C. (2014). Silicon nanowire-based devices for gas-phase sensing. Sensors *14*, 245–271. https://doi.org/10.3390/s140100245.

Chen, H., Liu, W., Zhu, A., Xiong, X., and Pan, J. (2017). Visible-light excited strong red emission of SnO_2 nanostructures. Mater.Res. Express *4*, 045019. https://doi.org/10.1088/2053-1591/aa6bbd.

Cheng, J.P., Wang, J., Li, Q.Q., Liu, H.G., and Li, Y. (2016). A review of recent developments in tin dioxide composites for gas sensing application. Ind. Eng. Chem. *44*, 1–22. https://doi.org/10.1016/j.jiec.2016.08.008.

Cho, B., Hahm, M.G., Choi, M., Yoon, J., Kim, A.R., Lee, Y.J., Park, S.G., Kwon, J.D., Kim, C.S., Song, M., and Jeong, Y. (2015). Charge-transfer-based gas sensing using atomic-layer MoS_2. Sci. Rep. *5*, 1–6. https://doi.org/10.1038/srep08052.

Cho, B., Kim, A.R., Kim, D.J., Chung, H.S., Choi, S.Y., Kwon, J.D., Park, S.W., Kim, Y., Lee, B.H., Lee, K.H., and Kim, D.H. (2016). Two-dimensional atomic-layered alloy junctions for high-performance wearable chemical sensor. ACS Appl. Mater. Inter. *8*, 19635–19642. https://doi.org/10.1021/acsami.6b05943.

Choi, Y.J., Hwang, I.S., Park, J.G., Choi, K.J., Park, J.H., and Lee, J.H. (2008). Novel fabrication of an SnO_2 nanowire gas sensor with high sensitivity. Nanotechnology *19*, 095508. https://doi.org/10.1088/0957-4484/19/9/095508.

Choi, S.Y., Kim, Y., Chung, H.S., Kim, A.R., Kwon, J.D., Park, J., Kim, Y.L., Kwon, S.H., Hahm, M.G., and Cho, B. (2017). Effect of Nb doping on chemical sensing performance of two-dimensional layered $MoSe_2$. ACS Appl. Mater. Inter. *9*, 3817–3823. https://doi.org/10.1021/acsami.6b14551.

Costa, I.M., Colmenares, Y.N., Pizani, P.S., Leite, E.R., and Chiquito, A.J. (2018). Sb doping of VLS synthesized SnO_2 nanowires probed by Raman and XPS spectroscopy. Chem. Phys. Lett. *695*, 125–130. https://doi.org/10.1016/j.cplett.2018.02.014.

Cui, H., Zheng, K., Xie, Z., Yu, J., Zhu, X., Ren, H., Wang, Z., Zhang, F., Li, X., Tao, L.Q., and Zhang, H. (2020). Tellurene nanoflake-based NO_2 sensors with superior sensitivity and a sub-parts-per-billion detection limit. ACS Appl. Mater. Inter. *12*, 47704–47713. https://doi.org/10.1021/acsami.0c15964.

Dey, A. (2018). Semiconductor metal oxide gas sensors: a review. Mater. Sci. Eng. B *229*, 206–217. https://doi.org/10.1016/j.mseb.2017.12.036.

Donarelli, M., and Ottaviano, L. (2018). 2D materials for gas sensing applications: a review on graphene oxide, MoS_2, WS_2 and phosphorene. Sensors *18*, 3638. https://doi.org/10.3390/s18113638.

Feng, P., Shao, F., Shi, Y., and Wan, Q. (2014). Gas sensors based on semiconducting nanowire field-effect transistors. Sensors *14*, 17406–17429. https://doi.org/10.3390/s140917406.

Gonzalez, J.M., and Oleynik, I.I. (2016). Layer-dependent properties of SnS_2 and $SnSe_2$ two-dimensional materials. Phys. Rev. B *94*, 125443. https://doi.org/10.1103/PhysRevB.94.125443.

Gu, D., Li, X., Zhao, Y., and Wang, J. (2017). Enhanced NO_2 sensing of SnO_2/SnS_2 heterojunction based sensor. Sens. Actuators B *244*, 67–76. https://doi.org/10.1016/j.snb.2016.12.125.

Han, Y., Huang, D., Ma, Y., He, G., Hu, J., Zhang, J., Hu, N., Su, Y., Zhou, Z., Zhang, Y., and Yang, Z. (2018). Design of hetero-nanostructures on MoS_2 nanosheets to boost NO_2 room-temperature sensing. ACS Appl. Mater. Inter. *10*, 22640–22649. https://doi.org/10.1021/acsami.8b05811.

Hao, J., Zhang, D., Sun, Q., Zheng, S., Sun, J., and Wang, Y. (2018). Hierarchical SnS_2/SnO_2nanoheterojunctions with increased active-sites and charge transfer for ultrasensitive NO_2 detection. Nanoscale *10*, 7210–7217. https://doi.org/10.1039/c8nr01379a.

Hellmich, W., Müller, G., Braunmühl, C.B., Doll, T., and Eisele, I. (1997). Field-effect-induced gas sensitivity changes in metal oxides. Sens. Actuators B *43*, 132–139. https://doi.org/10.1016/S0925-4005(97)00195-0.

Henning, A., Molotskii, M., Swaminathan, N., Vaknin, Y., Godkin, A., Shalev, G., and Rosenwaks, Y. (2015). Electrostatic limit of detection of nanowire-based sensors. Small *11*, 4931–4937. https://doi.org/10.1002/smll.201500566.

Jiang, J., Wong, C.P.Y., Zou, J., Li, S., Wang, Q., Chen, J., Qi, D., Wang, H., Eda, G., Chua, D.H., and Shi, Y. (2017). Two-step fabrication of single-layer rectangular SnSe flakes. 2D Mater. *4*, 021026. https://doi.org/10.1088/2053-1583/aa6aec.

Kang, M.J., Kim, J.Y., Seo, J., Lee, S., Park, C., Song, S.M., Kim, S.S., and Hahm, M.G. (2019). Atomic-layered tungsten diselenide-based porous 3D architecturing for highly sensitive chemical sensors. Phys. Status Solidi *13*, 1900340. https://doi.org/10.1002/pssr.201900340.

Khan, M.A.H., Debnath, R., Motayed, A., and Rao, M.V. (2021). Back-gate GaN nanowire-based FET device for enhancing gas selectivity at room temperature. Sensors *21*, 624. https://doi.org/10.3390/s21020624.

Kolmakov, A., Klenov, D.O., Lilach, Y., Stemmer, S., and Moskovitst, M. (2005). Enhanced gas sensing by individual SnO_2 nanowires and nanobelts functionalized with Pd catalyst particles. Nano Lett. *5*, 667–673. https://doi.org/10.1021/nl050082v.

Kumar, R., Zheng, W., Liu, X., Zhang, J., and Kumar, M. (2020). MoS_2-based nanomaterials for room-temperature gas sensors. Adv. Mater. Technol. *5*, 1901062. https://doi.org/10.1002/admt.201901062.

Lee, E., Yoon, Y.S., and Kim, D.J. (2018). Two-dimensional transition metal dichalcogenides and metal oxide hybrids for gas sensing. ACS Sens. *3*, 2045–2060. https://doi.org/10.1021/acssensors.8b01077.

Li, H., Yin, Z., He, Q., Li, H., Huang, X., Lu, G., Fam, D.W.H., Tok, A.I.Y., Zhang, Q., and Zhang, H. (2012). Fabrication of single-and multilayer MoS_2 film-based field-effect transistors for sensing NO at room temperature. Small *8*, 63–67. https://doi.org/10.1002/smll.201101016.

Li, R., Jiang, K., Chen, S., Lou, Z., Huang, T., Chen, D., and Shen, G. (2017). SnO_2/SnS_2 nanotubes for flexible room-temperature NH_3 gas sensors. RSC Adv. *7*, 52503–52509. https://doi.org/10.1039/c7ra10537a.

Liu, W., Gu, D., and Li, X. (2021). AuPt Bimetal-Functionalized $SnSe_2$ microflower-based sensors for detecting sub-ppm NO_2 at low temperatures. ACS Appl. Mater. Inter. *13*, 20336–20348. https://doi.org/10.1021/acsami.1c02500.

Li, X., Liu, W., Huang, B., Liu, H., and Li, X. (2020). Layered $SnSe_2$ microflakes and $SnSe_2$/SnO_2 heterojunctions for low-temperature chemiresistive-type gas sensing. J. Mater. Chem. C *8*, 15804–15815. https://doi.org/10.1039/d0tc02589e.

Lu, D., Yue, C., Luo, S., Li, Z., Xue, W., Qi, X., and Zhong, J. (2021). Phase controllable synthesis of SnSe and $SnSe_2$ films with tunable photoresponse properties. Appl. Surf. Sci. *541*, 148615. https://doi.org/10.1016/j.apsusc.2020.148615.

Matysiak, W., Tański, T., Smok, W., and Polishchuk, O. (2020). Synthesis of hybrid amorphous/crystalline SnO_2 1D nanostructures: investigation of morphology, structure, and optical properties. Sci. Rep. *10*, 1–10. https://doi.org/10.1038/s41598-020-71383-2.

McAlpine, M.C., Ahmad, H., Wang, D., and Heath, J.R. (2007). Highly ordered nanowire arrays on plastic substrates for ultrasensitive flexible chemical sensors. Nat. Mater. *6*, 379–384. https://doi.org/10.1038/nmat1891.

Moumen, A., Konar, R., Zappa, D., Teblum, E., Perelshtein, I., Lavi, R., Ruthstein, S., Nessim, G.D., and Comini, E. (2021). Robust room-temperature NO_2 sensors from exfoliated 2D few-layered CVD-grown bulk tungsten di-selenide (2H-WSe_2). ACS Appl. Mater. Inter. *13*, 4316–4329. https://doi.org/10.1021/acsami.0c17924.

Paolucci, V., D'Olimpio, G., Kuo, C.N., Lue, C.S., Boukhvalov, D.W., Cantalini, C., and Politano, A. (2020). Self-assembled SnO_2/$SnSe_2$ heterostructures: a suitable platform for ultrasensitive NO_2 and H_2 sensing. ACS Appl. Mater. Inter. *12*, 34362–34369. https://doi.org/10.1021/acsami.0c07901.

Ping, J., Fan, Z., Sindoro, M., Ying, Y., and Zhang, H. (2017). Recent advances in sensing applications of two-dimensional transition metal dichalcogenide nanosheets and their composites. Adv. Funct. Mater. *27*, 1605817. https://doi.org/10.1002/adfm.201605817.

Rai, R.K., Islam, S., Roy, A., Agrawal, G., Singh, A.K., Ghosh, A., and Ravishankar, N. (2019). Morphology controlled synthesis of low bandgap $SnSe_2$ with high photodetectivity. Nanoscale *11*, 870–877. https://doi.org/10.1039/c8nr08138g.

Ricciardella, F., Vollebregt, S., Polichetti, T., Miscuglio, M., Alfano, B., Miglietta, M.L., Massera, E., Di Francia, G., and Sarro, P.M. (2017). Effects of graphene defects on gas sensing properties towards NO_2 detection. Nanoscale *9*, 6085–6093. https://doi.org/10.1039/c7nr01120b.

Shalev, G. (2017). The electrostatically formed nanowire: a novel platform for gas-sensing applications. Sensors (Basel) *17*. https://doi.org/10.3390/s17030471.

Shao, X., Li, S., and Tang, D.M. (2018). Flaky nano-crystalline $SnSe_2$ thin films for photoelectrochemical current generation. RSC Adv. *8*, 32157–32163. https://doi.org/10.1039/c8ra04639e.

Shehada, N., Bronstrup, G., Funka, K., Christiansen, S., Leja, M., and Haick, H. (2015). Ultrasensitive silicon nanowire for real-world gas sensing: noninvasive diagnosis of cancer from breath volatolome. Nano Lett. *15*, 1288–1295. https://doi.org/10.1021/nl504482t.

Sun, Y.F., Liu, S.B., Meng, F.L., Liu, J.Y., Jin, Z., Kong, L.T., and Liu, J.H. (2012). Metal oxide nanostructures and their gas sensing properties: a review. Sensors *12*, 2610–2631. https://doi.org/10.3390/s120302610.

Thang, N.T., Thoan, N.H., Hung, C.M., Van Duy, N., Van Hieu, N., and Hoa, N.D. (2020). Controlled synthesis of ultrathin MoS_2 nanoflowers for highly enhanced NO_2 sensing at room temperature. RSC Adv. *10*, 12759–12771. https://doi.org/10.1039/D0RA00121J.

Vemula, M., Veeralingam, S., and Badhulika, S. (2021). Hybrid 2D/0D $SnSe_2$-SnO_2 vertical junction based high performance broadband photodetector. J. Alloy. Compd. *883*, 160826. https://doi.org/10.1016/j.jallcom.2021.160826.

Wang, C., Yin, L., Zhang, L., Xiang, D., and Gao, R. (2010). Metal oxide gas sensors: sensitivity and influencing factors. Sensors *10*, 2088–2106. https://doi.org/10.3390/s100302088.

Wang, T., Wang, Y., Sun, Q., Zheng, S., Liu, L., Li, J., and Hao, J. (2021). Boosted interfacial charge transfer in SnO_2/$SnSe_2$ heterostructures: toward ultrasensitive room-temperature H_2S detection. Inorg. Chem. Front. *8*, 2068–2077. https://doi.org/10.1039/d0qi01326a.

Yan, W., Lv, C., Zhang, D., Chen, Y., Zhang, L., Ó Coileáin, C., Wang, Z., Jiang, Z., Hung, K.M., Chang, C.R., and Wu, H.C. (2020). Enhanced NO_2 sensitivity in Schottky-contacted n-type SnS_2 gas

sensors. ACS Appl. Mater. Inter. *12*, 26746–26754. https://doi.org/10.1021/acsami.0c07193.

Yan, W., Worsley, M.A., Pham, T., Zettl, A., Carraro, C., and Maboudian, R. (2018). Effects of ambient humidity and temperature on the NO_2 sensing characteristics of WS_2/graphene aerogel. Appl. Surf. Sci. *450*, 372–379. https://doi.org/10.1016/j.apsusc.2018.04.185.

Zhao, S., Li, Z., Wang, G., Liao, J., Lv, S., and Zhu, Z. (2018). Highly enhanced response of MoS_2/porous silicon nanowire heterojunctions to NO_2 at room temperature. RSC Adv. *8*, 11070–11077. https://doi.org/10.1039/c7ra13484c.

Zhang, Y., Shi, Y., Wu, M., Zhang, K., Man, B., and Liu, M. (2018). Synthesis and surface-enhanced Raman scattering of ultrathin $SnSe_2$ nanoflakes by chemical vapor deposition. Nanomaterials *8*, 515. https://doi.org/10.3390/nano8070515.

Zhang, D., Wu, J., Li, P., and Cao, Y. (2017). Room-temperature SO_2 gas-sensing properties based on a metal-doped MoS_2 nanoflower: an experimental and density functional theory investigation. J. Mater. Chem. A *5*, 20666–20677. https://doi.org/10.1039/C7TA07001B.

Zhou, X., Gan, L., Tian, W., Zhang, Q., Jin, S., Li, H., Bando, Y., Golberg, D., and Zhai, T. (2015). Ultrathin $SnSe_2$ flakes grown by chemical vapor deposition for high-performance photodetectors. Adv. Mater. *27*, 8035–8041. https://doi.org/10.1002/adma.201503873.

STAR★METHODS

KEY RESOURCES TABLE

REAGENT or RESOURCE	SOURCE	IDENTIFIER
Chemicals, peptides, and recombinant proteins		
Sn powder	Sigma Aldrich	CAS: 7440-31-5
Se powder	Sigma Aldrich	CAS: 7782-49-2
Au pellet	RNDKOREA	http://www.rndkorea.co.kr/
Pt pellet	RNDKOREA	http://www.rndkorea.co.kr/
Ti pellet	RNDKOREA	http://www.rndkorea.co.kr/
Software and algorithms		
Origin	2018	www.originlab.com
Adobe illustrator	CC 2020	www.adobe.com
Adobe photoshop	CC 2020	www.adobe.com
Cinema 4D	2019	www.mawon.net
Other		
Optical microscopy	Olympus	BX53M
Raman spectroscopy	HORIBA Jobin Yvon	LabRAM Revolution
X-ray diffraction	PANalytical B.V.	Pro MRD
X-ray photoelectron spectroscopy	Thermo Fisher Scientific	K-Alpha
Field emission scanning electron microscopes	Hitachi	S-4300SE

RESOURCE AVAILABILITY

Lead contact

Further information requests should be directed to the lead contact, Myung Gwan Hahm (mghahm@inha.ac.kr).

Materials availability

This study did not generate new unique reagents. All the materials and methods used for the generation of data and analysis are mentioned in the manuscript.

Data and code availability

This Data used in this paper will be shared by the lead contact upon request. This paper does not report original code. Any additional information required to reanalyze the data reported in this paper is available from the lead contact upon request.

EXPERIMENTAL MODEL AND SUBJECT DETAILS

Our study does not use experimental models typical in the life sciences.

METHOD DETAILS

Synthesis of SnO_2 nanowires

Networked SnO_2 nanowires were grown using a vapor-liquid-solid (VLS) method. For the growth of the nanowires, a photolithography method was used first, and a trilayered-interdigitated electrode (50-nm-thick Ti, 200-nm-thick Pt and 3-nm-thick Au) was sequentially deposited on the SiO_2-grown Si (300 nm) substrates through sputtering. Next, the substrates were put into a horizontal quartz tube furnace on top of an Al_2O_3 crucible with high-purity (99.9%) metallic Sn powder as a source. The furnace was heated to 900°C for 30 min in Ar (300 sccm) and O_2 (10 sccm) gas flows, and the SnO_2 nanowires were selectively grown on the substrates.

Preparation of 1D SnO_2 – 2D $SnSe_2$ hybrid nanowire network

Ultrathin $SnSe_2$ was synthesized on the surface of the as-prepared SnO_2 nanowire network by CVD. A quartz tube was evacuated by a mechanical pump and flushed with 5% H_2-balanced Ar gas. The reaction was carried out at 550°C for 30 min using Se powder as the Se precursor.

Material characterization

XRD (Pro MRD) was conducted to confirm the crystal structure of the 1D SnO_2 – 2D $SnSe_2$ hybrid nanowire network. The Raman spectra of the pristine SnO_2 nanowires before and after the selenization process were obtained by Raman spectroscopy (LabRAM Revolution, HORIBA Jobin Yvon) with a 532-nm green laser. The valence state of each element of the as-prepared 1D SnO_2 – 2D $SnSe_2$ heterostructure was confirmed by XPS (K-Alpha, Thermo Scientific). The microstructure of the 1D SnO_2 – 2D $SnSe_2$ hybrid nanowire network was characterized by FESEM (S-4300SE, Hitachi) and FETEM (JEM-2100F, JEOL).

Gas sensing studies

For measuring the sensing performance, the gas sensor was electrically connected to an electrical measuring system that was interfaced with a computer. The sensors were placed in a horizontal tube furnace, and the temperature was measured in the range of 25–200°C. The desired concentration of the target gas was controlled in the gas chamber through mass flow controllers. To reduce any possible variation in the sensing properties, the total flow rate was fixed at 500 sccm. The resistances of the sensors were measured in air (R_a) and in the presence of the target gas (R_g), and the sensor response was defined as $S = R_g/R_g$ in oxidation gas and R_g/R_g in reducing gas. The response and recovery times were estimated as the time required to reach 90% of the saturated resistance after the NO_2 gas injection and removal, respectively.

QUANTIFICATION AND STATISTICAL ANALYSIS

Our study does not include statistical analysis or quantification.

ADDITIONAL RESOURCES

Our study has not generated or contributed to a new website/forum or if it is not part of a clinical trial.